Three New Isostructural Metal-organic Coordination Polymers from Triangular Pyridinedicarboxylate Ligand: Syntheses, Structures and Properties①

ZHU Ling-Bin[a, b] LI Fei[b] SUN Ming-Ling[b]
QIN Ye-Yan[b] YAO Yuan-Gen[b②]

[a] (*College of Chemistry and Material Science, Fujian Normal University, Fuzhou* 350007, *China*)

[b] (*Key Laboratory of Coal to Ethylene Glycol and Its Related Technology, Fujian Institute of Research on the Structure of Matter, Fujian Institute of Research on the Structure of Matter, Fuzhou* 350002, *China*)

ABSTRACT Three new isostructural coordination polymers, namely, $[Mg(cpna)(H_2O)_2]_n$ (**1**), $[Mn(cpna)(H_2O)_2]_n$ (**2**) and $[Co(cpna)(H_2O)_2]_n$ (**3**) (H_2cpna = 5-(3-carboxylphenyl)nicotic acid) are reported. They were synthesized by hydrothermal reactions of transition metal or alkaline earth metal chloride with 5-(3-carboxylphenyl)nicotic acid, respectively. Complexes **1**～**3** exhibit 2D layers with a 3,3-connected topology with Schläfli symbol $\{4.8^2\}$. Such layers including hexagonal rings and a quadrangular ring are further extended into an ordered 3D framework by hydrogen bonds between the $cpna^{2-}$ ligands and water molecules. The rare complex **1** has excellent luminescence and can be used as luminescent materials, while **2** and **3** possess prominent magnetism with potential applications in magnetic materials.

Keywords: isostructural polymer, 2D layers, 3D framework, hydrogen bonds, luminescence, magnetism;
DOI: 10.14102/j.cnki.0254–5861.2011–3078

1 INTRODUCTION

Functional coordination chemistry is based on molecular basis, and molecular design and assembly are used to construct functional coordination complexes. The potentials for use in photoelectricity[1], catalysis[2], adsorption[3-5], nonlinear optics[6] and magnetism[7] are also discussed. In recent years, with the improvement of synthesis and measurement technology, the theory of crystallography has become more and more mature. The simple nitrogen-containing ligands and their derivatives such as imidazole and triazole have not been able to meet the needs of developing new complexes. It is noted that much attention has been paid to the coordination polymers that are assembled by polycarboxylic acids and N-heterocyclic ligands. The spacer of these aromatic multi-carboxylate ligands sometimes plays an important role in forming the final structure of the molecule due to their varied coordination capability[8]. For example, Liang et al. synthesized a heterometal complex $\{[Gd_2Cu_3(pydc)_6(H_2O)]\cdot 4H_2O\}_n$ by reacting 2,5-pyridinedicarboxylic acid with copper and rare earth metal ions under hydrothermal conditions[9], and Lahoud et al. used 1H-pyrazole-3,5-dicarboxylicacid and various rare earth metal ions to synthesize rare earth complexes[10]. However, studies engaged in 5-(3-carboxylphenyl)nicotic acid are less[11-14]. We delved into the construction and properties of the complexes derived from pyridyl carboxylic ligands. Due to the coordination of metals and ligands, the emission wavelength of organic ligand will be significantly affected. Therefore, the luminescent properties can be controlled by changing metal ions, organic ligands, synthetic methods and conditions, etc., so that a specific luminescent material can be obtained[15]. By means of crystal engineering, one can obtain a coordination polymer with improved magnetic properties or other useful properties by controlling the position and connection of the spin-bearing center magnetic properties or other useful properties by controlling the position and connection of the spin-bearing center[13].

Received 25 December 2020; accepted 5 February 2021 (**CCDC 1900827-1900829**)

① This research was supported by the National Natural Science Foundation of China (21703247) and the Science Foundation of Fujian Province (2018J05029, 2019J05156, 2019H0053)

② Corresponding author. E-mail: yyg@fjirsm.ac.cn

In this work, we have been continuing our efforts in the self-assembly and characterization of new metal assemblies based on 5-(3-carboxylphenyl)nicotic acid ligand. H_2cpna contains both nitrogen and carboxylate groups and can be used in a variety of coordination modes. Since the polycarboxylic groups can be deprotonated in whole or in part, they can serve as a donor or acceptor of a hydrogen bond, contributing to the formation of a supramolecular structure. In recent years, compared with transition metals and rare earth metals, MOFs based on alkaline earth metal construction have also been reported, but there are still few, so not only the transition metal salt (Co^{2+} and Mn^{2+}) but also the alkaline earth metal salt (Mg^{2+}) were used to synthesize complexes with the ligand H_2cpna.

Herein, we report the successful self-assembly of three new isostructural complexes: $Mg(cpna)(H_2O)_2$ (**1**), $Mn(cpna)(H_2O)_2$ (**2**), and $Co(cpna)(H_2O)_2$ (**3**), which exhibit 2-fold structures with a short symbol of $\{4.8^2\}$ and then extend into 3D frameworks by hydrogen bonds. Since these three complexes are isostructural, we only list the molecular structural formula of complex **1** as a representative (Scheme 1). All complexes were characterized by single-crystal X-ray diffraction, topological analyses, infrared spectra, elemental analyses and thermogravimetric analyses. In addition, the photo-luminescence of complex **1** was discussed in detail, while magnetic properties of complexes **2** and **3** were also studied.

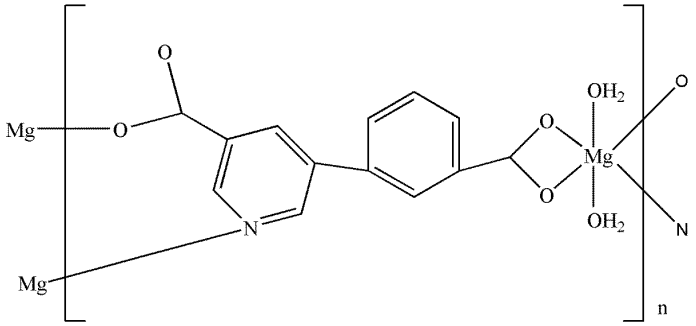

Complex **1**

Scheme 1

Scheme 1. Cordination mode of $cpna^{2-}$ in complex 1

2 EXPERIMENTAL

All raw materials were purchased through commercial channels and not purified. Elemental analyses (C, H, N) were measured on an EA1110 CHNS-0 CE elemental analyzer. Infrared spectroscopy was performed on a Nicolet Magna 750 FT-IR spectrometer with KBr pellets at 400～4000 cm^{-1}. Powder X-ray diffraction data (PXRD) were collected on a Rigaku MiniFlex II diffractometer with Cu$K\alpha$ radiation (λ = 1.54056 Å). Thermal gravimetric analyses (TGA) were determined on a NETSCHZ STA-449C thermal analyzer from room temperature to 800 ^oC under nitrogen atmosphere at a heating rate of 10 ^oC min. The luminescence spectra were measured on a FLS920 luminescence spectrophotometer at room temperature by powdered solid samples. The magnetic measurements were made with a commercial quantum design physical property measurement system (PPMS).

2. 1 Syntheses and crystallization

2. 1. 1 Synthesis of $[Mg(cpna)(H_2O)_2]_n$ (1)

$MgCl_2$ 2.5H_2O (0.046 g, 0.2 mmol) and H_2cpna (0.049 g, 0.2 mmol) were dissolved in 8 mL of deionized water, then 10 uL of acetonitrile was added, stirred for 30 minutes, placed in a 25 mL stainless-steel autoclave lined with polytetrafluoroethylene tubes, and crystallized at 140 ℃ for 90 h. Then, it was cooled to room temperature, and the crystals were filtered and washed with distilled water. It was cooled to obtain a pure phase of colorless rod crystals of **2** in a yield of 58% (by Mg). Anal. Calcd. for $C_{13}H_{11}MgNO_6$: C, 51.78; H, 3.68; N, 4.65%. Found: C, 51.31; H, 3.82; N, 4.33%. IR (KBr pellet, cm^{-1}): 3374(m), 3294(m), 3080(m), 2900(s), 1615(s), 1544(s), 1425(s), 1377(s), 917(m), 863(m), 768(s), 712(s), 419(m).

2. 1. 2 Synthesis of $[Mn(cpna)(H_2O)_2]_n$ (2)

The synthesis method of complex **2** is the same as that of **1**, except that $MgCl_2$ 2.5H_2O is replaced by $MnCl_2$ ·4H_2O. It was cooled to obtain a pure phase of white rod crystals of **2** in a

yield of 49% (by Mn). Anal. Calcd. for $C_{13}H_{11}MnNO_6$: C, 47.01; H, 3.34; N, 4.22%. Found: C, 47.05; H, 3.30; N, 4.18%. IR (KBr pellet, cm^{-1}): 3349(m), 3238(m), 3088(m), 1615(s), 1615(s), 1409(s), 1369(s), 871(m), 775(m), 704(s), 585(m), 427(m).

2. 1. 3 Synthesis of $[Co(cpna)(H_2O)_2]_n$ (3)

The synthesis method of complex **3** is the same as that of complex **1**, except that $MgCl_2·2.5H_2O$ is replaced by $CoCl_2·4H_2O$. It was cooled to obtain a pure phase of red rod crystals of **3** in 52% yield (by Co). Anal. Calcd. for $C_{13}H_{11}CoNO_6$: C, 46.45; H, 3.30; N, 4.17%. Found: C, 46.66; H, 3.35; N, 4.12%. IR (KBr pellet, cm^{-1}): 3373(m), 3254(m), 3104(m), 1615(s), 1552(s), 1432(s), 1377(s), 847(m), 767(s), 712(s), 569(s), 427(s).

2. 2 Refinement

Crystal data, data collection and structure refinement details are summarized in Table 1. The data were collected using a computer-controlled Oxford Xcalibur E diffractometer with graphite-monochromatic Mo$K\alpha$ radiation ($\lambda_{MoK\alpha}$ = 0.71073 Å) at 298(2) K. The final unit cell parameters were derived by global refinements of reflections obtained from integration of all the frame data. Empirical absorption corrections were applied using the SADABS program. The structure was solved by direct methods using the SHELXS program and refined by full-matrix least-squares techniques SHELXL on F^2[16]. Hydrogen atoms were located using the geometric method. Non-hydrogen atoms were refined with anisotropic thermal parameters. The SQUEEZE option of PLATON could eliminate disordered guest molecules[17].

Table 1. Summary of Crystal Data and Structure Refinements for 1～3

	1	**2**	**3**
Chemical formula	$C_{13}H_{11}MgNO_6$	$C_{13}H_{11}MnNO_6$	$C_{13}H_{11}CoNO_6$
M_r	301.54	332.17	336.16
Crystal system, space group	Monoclinic, $P2_1/c$	Monoclinic, $P2_1/c$	Monoclinic, $P2_1/c$
a, b, c (Å)	13.4566(4), 11.8575(4), 7.7031(3)	13.5539(4), 11.9453(3) 7.8035(2)	13.3887(5), 11.8184(5) 7.7360(3)
β (°)	98.186(3)	98.510(3)	98.246(4)
Z	4	4	4
Radiation type	Mo$K\alpha$	Mo$K\alpha$	Mo$K\alpha$
V (Å^3)	1216.60(7)	1249.52(6)	1211.44(8)
μ (mm^{-1})	0.18	1.09	1.45
Crystal size (mm)	0.25 × 0.12 × 0.07	0.19 × 0.10 × 0.07	0.25 × 0.10 × 0.08
T_{min}, T_{max}	0.975, 0.988	0.878, 0.927	0.841, 0.891
No. of measured, independent and observed	5011, 2383, 1813	4847, 2544, 2270	5037, 2511, 2229
R_{int}	0.027	0.026	0.025
$(\sin\theta/\lambda)_{max}$ (Å^{-1})	0.645	1.356	0.680
R ($F^2 > 2\sigma(F^2)$)^a, $wR(F^2)^b$, S	0.042, 0.101, 1.071	0.048, 0.146, 1.065	0.047, 0.151, 1.030
No. of reflections	2383	2480	2509
No. of parameters	196	192	199
No. of restraints	0	0	0
H-atom treatment	H atoms treated by a mixture of independent and constrained refinement	H-atom parameters constrained	H atoms treated by a mixture of independent and constrained refinement
$\Delta\rho_{max}$, $\Delta\rho_{min}$ (e·Å^{-3})	0.32, –0.34	0.46, –0.61	1.22, –0.43

$^aR = \Sigma||F_o| - |F_c||/\Sigma|F_o|$, $^bwR = [\Sigma[w(F_o^2 - F_c^2)^2]/\Sigma w(F_o^2)^2]^{1/2}$

3 RESULTS AND DISCUSSION

3. 1 Crystal structures

Single-crystal X-ray diffraction reveals that complexes **1**～**3** are all isostructural. They crystallize in monoclinic space group $P2_1/c$. For the sake of simplicity, herein, we only describe the structure of complex **1** in detail, and other structures of complexes are shown in Fig. S1. As shown in Fig. 1, unit of **1** includes an independent Mg^{2+} center, a fully deprotonated H_2cpna ligand, and two water molecules. All Mg(II) ions in **1** are equivalent, and the coordination environment around the central Mg(II) ion is shown in Fig. 2. The central Mg(II) ion is in a slightly distorted octahedral coordination sphere, coordinating with one nitrogen atom

(N(1)^{ii}) and three oxygen atoms (O(1), O(2), O(3)^{i}) from three different cpna molecules (Mg−N(1)^{ii} 2.239(2) Å, Mg(1)−O(1) 2.208(2) Å, Mg(1)−O(2) 2.161(2) Å and Mg(1)−O(3)^{i} 2.024(3) Å) and with two oxygen atoms (O(1W), O(2W)) from two H_2O molecules (Mg(1)−O(1W) 2.086(4) Å and Mg(1)−O(2W) 2.043(8) Å). All bonds are consistent with the literature reports[18]. The L−Mg(1)−L (L = O, N) bond angles range from 88.36(7)° to 174.47(8)°, which are listed in Table 2 in detail. The H_2cpna ligand removes hydrogen from the two carboxyl groups during coordination process and bridge two Mg(II) ions and displays two coordination modes (μ_2-η^1:η^1 and μ_1-η^1:η^0). Owing to the coordination of cpna^{2-} ligands with Mg^{2+} metal, both the pyridyl and phenyl rings in the cpna^{2-} ligands are distorted and the dihedral angle between two aromatic rings of the cpna^{2-} is 25.62° (Fig. 2a). In the asymmetric unit **1**, the two cpna^{2-} ligands adopt a μ_3-η^1:η^1:η^1 bridging mode to connect two neighboring Mg(II) ions, fabricating a coplanar quadrangular ring, and four Mg(II) are linked by four cpna^{2-} ligands to form a non-planar octagonal boat-like ring. Both quadrangular rings and octagonal rings are spaced apart to result in a unique 2D network layer (Fig. 2b).

Table 2. Selected Bond Lengths (Å) and Bond Angles (°) for Complex 1

Bond	Dist.	Bond	Dist.	Bond	Dist.
Mg(1)−O(3)^{i}	2.0243(16)	Mg(1)−O(2W)	2.0438(19)	Mg(1)−O(1W)	2.0864(18)
Mg(1)−O(2)	2.1611(17)	Mg(1)−O(1)	2.2082(15)	Mg(1)−N(1)^{ii}	2.239(2)
Angle	(°)	Angle	(°)	Angle	(°)
O(3)^{i}−Mg(1)−O(2W)	91.80(8)	O(3)^{i}−Mg(1)−O(1W)	90.16(7)	O(2W)−Mg(1)−O(1W)	174.47(8)
O(3)^{i}−Mg(1)−O(2)	88.36(7)	O(2W)−Mg(1)−O(2)	92.25(7)	O(1W)−Mg(1)−O(2)	92.97(7)
O(3)^{i}−Mg(1)−O(1)	148.21(7)	O(2W)−Mg(1)−O(1)	92.27(7)	O(1W)−Mg(1)−O(1)	88.77(7)
O(2)−Mg(1)−O(1)	59.99(6)	O(3)^{i}−Mg(1)−N(1)^{ii}	122.54(7)	O(2W)−Mg(1)−N(1)^{ii}	85.12(8)
O(1W)−Mg(1)−N(1)^{ii}	89.46(7)	O(2)−Mg(1)−N(1)^{ii}	149.01(6)	O(1)−Mg(1)−N(1)^{ii}	89.22(6)

Symmetry codes: (i) *x*+1, –*y*+1/2, *z*+1/2; (ii) –*x*, –*y*+1, –*z*

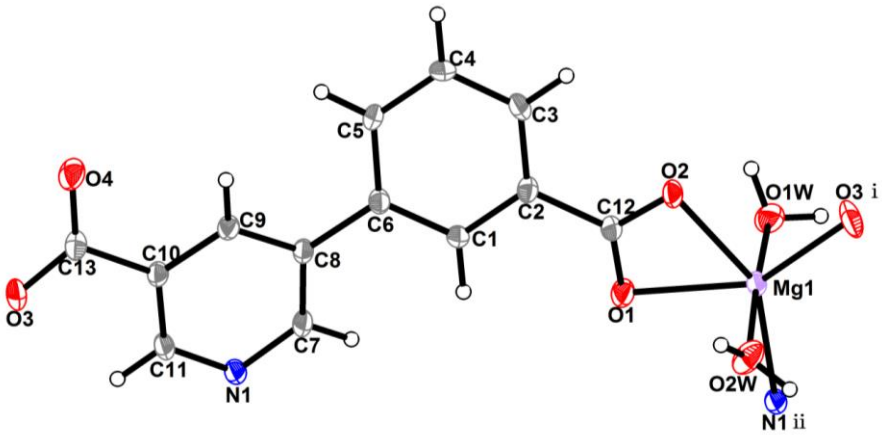

Fig. 1. Perspective view of the coordination environment of the Mg(II) atom in 1 with 50% thermal ellipsoids. Symmetry codes: (i) *x*+1, –*y*+1/2, *z*+1/2; (ii) –*x*, –*y*+1, –*z*; (iii) *x*–1, –*y*+1/2, *z*–1/2

In order to more directly understand the framework of complex **1**, we apply the method of topology analysis to reduce the multidimensional structure to simple nodes and linkers. Each cpna^{2-} is connected to three Mg(II) ions and each Mg^{2+} is surrounded by three cpna^{2-} liands, so both cpna^{2-} and Mg^{2+} can be simplified as 3-connected nodes. The overall structure of **1** can be rationalized as a 3,3-connected topology with Schläfli symbol {4.8^2} (Fig. 2c).

Interestingly, the 2D layers are extended into an ordered 3D framework by hydrogen bonds between the cpna^{2-}ligands (C(11)–H(11)···O(4)^{viii}: 3.284(3) Å, 145°), in which C atoms are from the pyridyl rings and O atoms are from the uncoordinated carboxylate groups of cpna^{2-} ligands, as well as a hydrogen bond (O(1W)–H(1WB)···O(2)^{v}: 2.841(2) Å, 153°; O(2W)–H(2WB)···O(2)^{vii}: 2.740(2) Å, 169°; O(1W)–H(1WA)···O(4)^{iv}: 2.833(2) Å, 141°; O(2W)–H(2WA)···O(4)^{vi}: 2.736(2) Å, 151°) between the coordinating water molecules and ligands, in which O atoms are from coordination water molecules and carboxylate groups of cpna^{2-} ligands, respectively (Fig. 2d). The detailed hydrogen bonds are listed in Table 3.

Table 3. Hydrogen Bonds for Complex 1 (Å and °)

D–H···A	D–H	H···A	D···A	D–H···A
O(1W)–H(1WA)···O(4)^{iv}	0.86	2.11	2.833(2)	141
O(1W)–H(1WB)···O(2)^{v}	0.86	2.04	2.841(2)	153
O(2W)–H(2WA)···O(4)^{vi}	0.85	1.96	2.736(2)	151
O(2W)–H(2WB)···O(2)^{vii}	0.81	1.95	2.740(2)	169
C(7)–H(7)···O(1)^{ii}	0.93	2.41	3.034(3)	124
C(11)–H(11)···O(4)^{viii}	0.93	2.48	3.284(3)	145

Symmetry codes: (ii) –*x*+1, –*y*, –*z*; (iv) –*x*+1, *y*–1/2, –*z*–1/2; (v) *x*, 1/2–*y*, –1/2+*z*; (vi) 1–*x*, –1/2+*y*, 1/2–*z*; (vii) *x*, 1/2–*y*, 1/2+*z*; (viii) –*x*, –1/2+*y*, –1/2–*z*

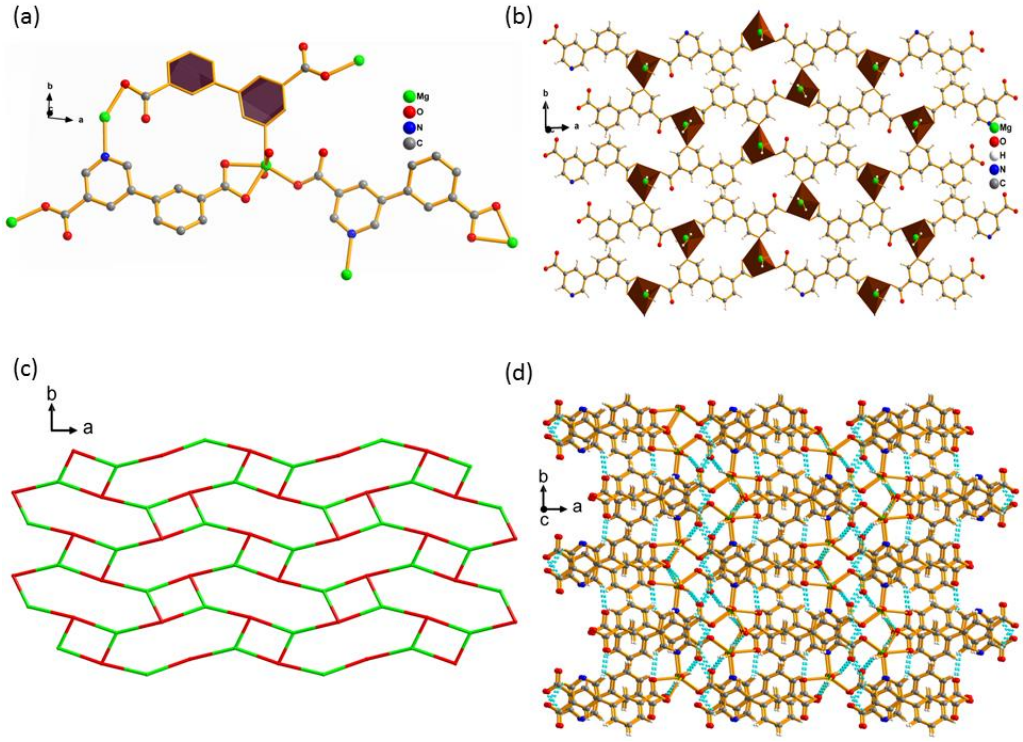

Fig. 2. (a) Dihedral angle between two aromatic rings of the cpna^{2-} is 25.62 °. (b) A polyhedral view of the 2D layer structure. (c) View of topological (4.8^2) net of the 2D layer. (d) 3D supramolecular framework constructed by hydrogen bonds

3. 2 IR, PXRD and TGA

The infrared spectra of complexes **1**～**3** show that the characteristic peaks of water molecule O–H are in the range of 3500～3300 cm^{-1}: 3374 cm^{-1} (**1**), 3349 cm^{-1} (**2**) and 3373 cm^{-1} (**3**). The absorption of phenyl ring hydrocarbon (At–H) is in the range of 3200～3000 cm^{-1}: 3080 cm^{-1} (**1**), 3088 cm^{-1} (**2**) and 3104 cm^{-1} (**3**). When the carboxyl group is coordinated with metal, the proton is removed, and the characteristic peak of the group disappears in the range of 1725～1700 cm^{-1}, as well as the characteristic absorption peaks of COO^{-} in the 1650～1440 cm^{-1} region: 1615 cm^{-1}, 1544 cm^{-1} (**1**), 1615 cm^{-1}, 1522 cm^{-1} (**2**), 1615 cm^{-1}, 1552 cm^{-1} (**3**) (Fig. S2). The above analyses are consistent with the X-ray diffraction results.

In order to better study the various properties of the complexes, their purity need to be characterized firstly. We performed powder X-ray diffraction (XRD) analyses on the three complexes synthesized, and found the XRD patterns of complexes **1** ～ **3** obtained by experiment are basically consistent with the simulated ones (Fig. S3-Fig. S5). The purity of these three complexes is high, and the related properties of them can be studied.

Complexes **1**～**3** are stable in air and maintain stable crystalline states at room temperature. To investigate the thermal stabilities of complexes **1** ～ **3**, we performed thermogravimetric analysis (TG). The thermal decomposition plots of compounds **1**～**3** are shown in Fig. S6. Complex **1** was thermal stable up to 102 °C, then lost 12.1% between 102 and 237 °C, corresponding to the decomposition of two H_2O molecules (calculated 11.9%). After that the H_2cpna ligands begin to decompose. The weight loss curves of complexes **2** and **3** are similar to **1**. In **2**, the departure of the coordinated water molecules of complex **2** occurs from 121 to 200 °C

(observed 10.8%, calculated 11.1%). Complex **3** loses two coordinated water molecules in 125～210 °C with the weight loss of 10.5% (calculated 10.7%).

3. 3 Luminescence of 1

Fluorescent coordination polymers (L-CPs) have attracted much attention due to their wide application prospects in lighting, sensing, and biological imaging[19, 20]. The researches on transition metal-based L-CPs based on rare earth ions and d^{10} electronic configuration is the most[21]. The special closed-shell electronic configuration of Mg(II) is coordinated with organic ligands without the loss of light energy caused by *d*-*d* transitions. It is very suitable for the construction of L-CPs based on the luminescence mechanism of organic ligands.

Luminescent properties of complex **1** at room temperature have been studied. It can be seen from Fig. 3, when excited at 275 nm, the free ligand H_2cpna and complex **1** have the largest emission peaks at 392 and 338 nm, respectively. According to literature reports, the luminescence of H_2cpna ligands can be attributed to the transition of $n\rightarrow\pi^*/\pi\rightarrow\pi^*$ within ligands[21]. It can also be seen from Fig. 3 that when the ligands form complex **1** with Mg ions, the emission intensity of **1** relative to the ligand is enhanced due to the increased rigidity of the ligand after coordinating with Mg^{2+}, which reduces the loss of non-radiative energy[22, 23]. At the same excitation wavelength (ex = 275 nm), the largest fluorescence emission peak of complex **1** is 338 nm. Compared to the free H_2cpna, the luminescence of complex **1** has certain blue shifts, resulting from the ligand centered charge transfer. It can also be concluded that the energy transfer process and phonon dynamics within the scintillators take place mainly in the same luminescence centre species, so the emission spectra of **1** remained similar when excited either by ionizing radiation or by nonionizing irradiation[24, 25].

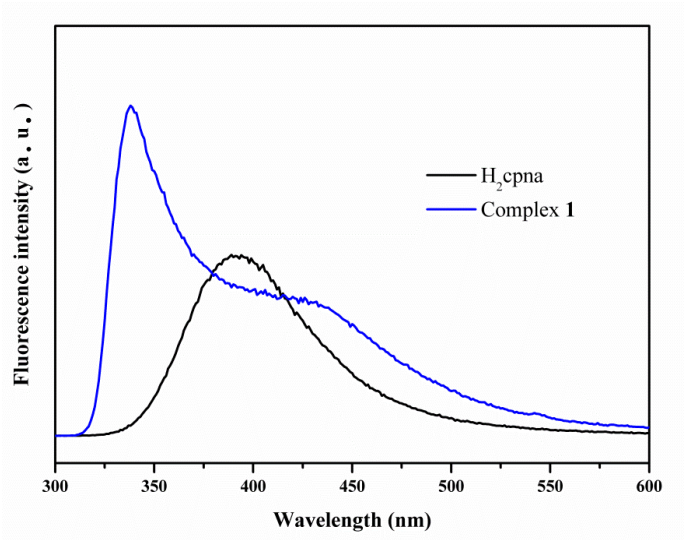

Fig. 3. Emission spectra of H_2cpna and complex 1

3. 4 Magnetic properties of 2 and 3

The magnetic susceptibility measurements for compounds **2** and **3** were performed with polycrystalline samples from 300 to 2 K under an applied field of 1000 Oe. For **2**, the χ_mT value is 4.36 $cm^3 \cdot mol^{-1} \cdot K$ at room temperature, which is very close to the value of 4.375 $cm^3 \cdot mol^{-1} \cdot K$ for an isolated Mn(Ⅱ) ion with g = 2.0. Upon cooling, the χ_mT remains constant to about 30 K, after which it decreases abruptly to a minimum value of 3.42 $cm^3 \cdot mol^{-1} \cdot K$ at 2 K, indicating the paramagnetic behavior. The paramagnetic behavior in **2** is also suggested by the very small Weiss constant θ = −0.25 K, obtained from the data of χ_m^{-1} *vs*. T in the temperature range of 20～300 K by Curie-Weiss law (Fig. 4). For **3**, the experimental χ_mT value at 300 K is 3.39 $cm^3 \cdot mol^{-1} \cdot K$, which is larger than that expected for non-interacting high-spin Co(II) ions (1.88 $cm^3 \cdot mol^{-1} \cdot K$ with g = 2.0). This divergence suggests that the orbital contribution of octahedral Co(Ⅱ) ions is involved. After further cooling, the χ_mT decreases continuously and reaches a minimum value of 1.80 $cm^3 \cdot mol^{-1} \cdot K$ at 2 K. From 2 to 300 K, the χ_m follows the Curie-Weiss law giving θ = –4.87 K and C = 3.45 $cm^3 \cdot mol^{-1} \cdot K$ (Fig. 5). Considering the structure of **3**, the negative Weiss constant may be caused by the spin-orbital coupling together with the zero-field splitting.

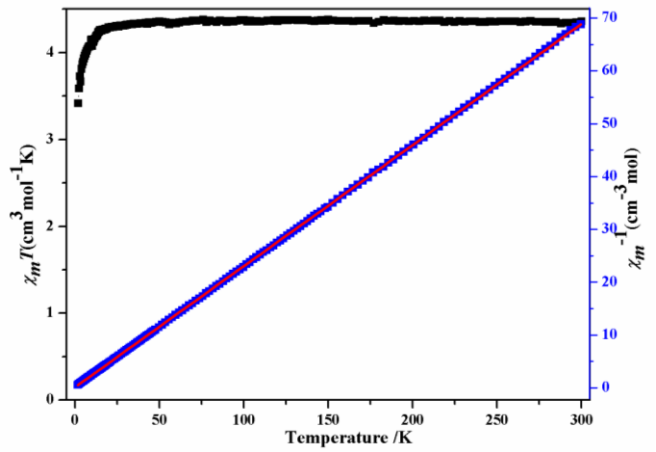

Fig. 4. $\chi_m T$ **and** χ_m^{-1} ***vs.*** ***T*** **curves measured under an applied field 1000 Oe for 2**

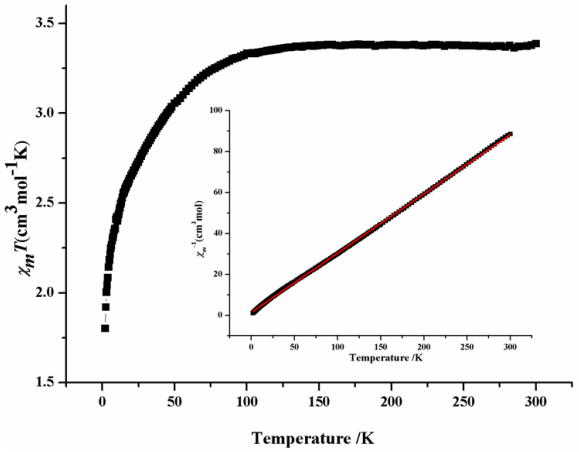

Fig. 5. $\chi_m T$ **and** χ_m^{-1} ***vs.*** ***T*** **curves measured under an applied field of 1000 Oe for 3**

4 CONCLUSION

In summary, we synthesized three novel isostructural complexes, namely, Mg(cpna)$(H_2O)_2$ (**1**), Mn(cpna)$(H_2O)_2$ (**2**) and Co(cpna)$(H_2O)_2$ (**3**), based on 5-(3-carboxylphenyl) nicotic acid (H_2dcpa) under hydrothermal conditions. Although the metal centers are different in three complexes, they exhibit the same structures because they are carried out under the same reaction conditions. Interestingly, all of them exhibit 2D layered structures with a short symbol of $\{4.8^2\}$ topology and ultimately stretch into 3D frameworks by hydrogen bonds. In addition, we have characterized the properties of these complexes. The rare complex **1** has excellent luminescence and it can be used as a potential luminescent material, while complexes **2** and **3** have pronounced magnetism and may be utilized as magnetic materials.

REFERENCES

(1) Hu, Z.; Deibert, B. J.; Li, J. Luminescent metal-organic frameworks for chemical sensing and explosive detection. *Chem. Soc. Rev.* **2014**, 43, 5815–5840.

(2) Dhakshinamoorthy, A.; Garcia, H. Metal-organic frameworks as solid catalysts for the synthesis of nitrogen-containing heterocycles. *Chem. Soc. Rev.* **2014**, 43, 5750–5765.

(3) He, Y.; Zhou, W.; Qian, G.; Chen, B. Methane storage in metal-organic frameworks. *Chem. Soc. Rev.* **2014**, 43, 5657–5678.

(4) Li, B.; Wen, H. M.; Zhou, W.; Chen, B. Porous metal-organic frameworks for gas storage and separation: what, how, and why? *J. Phys. Chem. Lett.* **2014**, 5, 3468–3479.

(5) Almasi, M.; Zelenak, V.; Gyepes, R.; Zauska, L.; Bourrelly, S. A series of four novel alkaline earth metal-organic frameworks constructed of Ca(II),

Sr(II), Ba(II) ions and tetrahedral MTB linker: structural diversity, stability study and low/high-pressure gas adsorption properties. *RSC ADV*. **2020**, 10, 32323–32334.

(6) He, Y. P.; Tan, Y. X.; Zhang, J. Gas sorption, second-order nonlinear optics, and luminescence properties of a series of lanthanide-organic frameworks based on nanosized tris((4-carboxyl)phenylduryl)amine ligand. *Inorg. Chem.* **2013**, 52, 12758–12762.

(7) Coronado, E.; Espallargas, G. M. Dynamic magnetic MOFs. *Chem. Soc. Rev.* **2013**, 42, 1525–1539.

(8) Gu, J. Z.; Cai, Y.; Wen, M.; Shi, Z. F.; Kirillov, A. M. A new series of Cd(II) metal-organic architectures driven by soft ether-bridged tricarboxylate spacers: synthesis, structural and topological versatility, and photocatalytic properties. *Dalton Trans*. **2018**, 47, 14327–14339.

(9) Liang, Y. C.; Cao, R.; Su, W. P.; Hong, M. C.; Zhang, W. J. Syntheses, structures, and magnetic properties of two gadolinium(III)-copper(II) coordination polymers by a hydrothermal reaction. *Angew. Chem. Int. Ed*. **2000**, 39, 3304–3307.

(10) Lahoud, M. G.; Muniz, E. C.; Arroyos, G.; Favaro, M. A.; Davolos, M. R.; D'Vries, R. F.; Ellena, J.; Freitas, R. S.; Arrighi, E.; Frem, RCG. Rare earth coordination dinuclear compounds constructed from 3,5-dicarboxypyrazolate and succinate intermetallic bridges. *New J. Chem.* **2016**, 40, 5338–5346.

(11) Hou, J. J.; Zhang, R.; Qin, Y. L.; Zhang, X. M. From (3,6)-connected kgd, chiral anh to (3,8)-connected tfz-d nets in low nuclear metal cluster-based networks with triangular pyridinedicarboxylate ligand. *Cryst. Growth Des*. **2013**, 13, 1618–1625.

(12) Wang, H. M.; Yang, Y. Y.; Zeng, C. H.; Chu, T. S.; Zhu, Y. M.; Ng, S. W. A highly luminescent terbium-organic framework for reversible detection of mercury ions in aqueous solution. *Photochem. Photobial. Sci*. **2013**, 12, 1700–1706.

(13) Han, Y.; Xu, H.; Liu, Y.; Li, H.; Hou, H.; Fan, Y.; Batten, S. R. Temperature-dependent capture of water molecules by saddle-shaped hexanuclear carboxylate cycloclusters in a (3,18)-connected metal-organic framework. *Chem. Eur. J*. **2012**, 18, 13954–13958.

(14) Liu, B.; Li, Y.; Hou, L.; Yang, G.; Wang, Y. Y.; Shi, Q. Z. Dynamic Zn-based metal-organic framework: stepwise adsorption, hysteretic desorption and selective carbon dioxide uptake. *J. Mater. Chem. A* **2013**, 1, 6535–6538.

(15) Chen, J.; Zhang, Q.; Liu, Z. F.; Wang, S. H.; Xiao, Y.; Li, R.; Xu, J. G.; Zhao, Y. P.; Zheng, F. K.; Guo, G. C. Color tunable and near white-light emission of two solvent-induced 2D lead(II) coordination networks based on a rigid ligand 1-tetrazole-4-imidazole-benzene. *Dalton Transactions*. **2015**, 44, 10089–10096.

(16) Sheldrick, G. M. Crystal structure refinement with SHELXL. *Acta Cryst. C* **2015**, 71, 3–8.

(17) Spek, A. L. PLATON SQUEEZE: a tool for the calculation of the disordered solvent contribution to the calculated structure factors. *Acta Cryst. C* **2015**, 71, 9–18.

(18) Biswas, A.; Kim, M. B.; Kim, S. Y.; Yoon, T. U.; Kim, S. I.; Bae, Y. S. A novel 3-D microporous magnesium-based metal-organic framework with open metal sites. *RSC Adv*. **2016**, 6, 81485–81490.

(19) Allendorf, M. D.; Bauer, C. A.; Bhakta, R. K.; Houk, R. J. T. Luminescent metal-organic frameworks. *Chem. Soc. Rev.* **2009**, 38, 1330–1352.

(20) Cui, Y.; Yue, Y.; Qian, G.; Chen, B. Luminescent functional metal-organic frameworks. *Chem. Rev.* **2012**, 112, 1126–1162.

(21) Heine, J.; Mueller-Buschbaum, K. Engineering metal-based luminescence in coordination polymers and metal-organic frameworks. *Chem. Soc. Rev.* **2013**, 42, 9232–9242.

(22) Fu, G.; He, Y.; Li, W.; Miao, T.; Lue, X.; He, H.; Liu, L.; Wong, W, Y. Efficient white polymer light-emitting diodes (WPLEDs) based on covalent-grafting of Zn-2(MP)(3)(OAc) into PVK. *Chem Sci*. **2020**, 11, 2640–2646.

(23) Son, H. J.; Han, W. S.; Chun, J. Y.; Kang, B. K.; Kwon, S. N.; Ko, J.; Han, S. J.; Lee, C.; Kim, S. J.; Kang, S. O. Generation of blue light-emitting zinc complexes by band-gap control of the oxazolyl phenolate ligand system: syntheses, characterizations, and organic light emitting device applications of 4-coordinated bis(2-oxazolylphenolate) zinc(II) complexes. *Inorg. Chem*. **2008**, 47, 5666–5676.

(24) Lu, J.; Wu, H. F.; Wang, W. F.; Xu, J. G.; Zheng, F. K.; Guo, G. C. Calcium-based efficient cathode-ray scintillating metal-organic frameworks constructed from pi-conjugated luminescent motifs. *Chem. Commun*. **2019**, 55, 13816–13819.

(25) Yan, Y.; Chen, J.; Zhang, N. N.; Wang, M. S.; Sun, C.; Xing, X. S.; Li, R.; Xu, J. G.; Zheng, F. K.; Guo, G. C. Grinding size-dependent mechanoresponsive luminescent Cd(II) coordination polymer. *Dalton Trans*. **2016**, 45, 18074–18078.